Theor Chem Account (2007) 118:915–922
DOI 10.1007/s00214-007-0372-9

REGULAR ARTICLE

A CASPT2//CASSCF study of the quartet excited state $\tilde{a}^4A''$ of the HCNN radical

Yang Liu · Xu-Ri Huang · Chia-Chung Sun

Received: 9 May 2007 / Accepted: 12 June 2007 / Published online: 19 July 2007

Abstract Complete active space self-consistent field and second-order multiconfigurational perturbation theory methods have been performed to investigate the quartet excited state $\tilde{a}^4A''$ potential energy surface of HCNN radical. Two located minima with respective *cis* and *trans* structures could easily dissociate to CH ($\tilde{a}^4\Sigma^-$) and $N_2(\tilde{X}^1\Sigma_g^+)$ products with similar barrier of about 16.0 kcal/mol. In addition, four minimum energy crossing points on a surface of intersection between $\tilde{a}^4A''$ and X ($X = \tilde{X}^2A''$ and $\tilde{A}^2A'$) states are located near to the minima. However, the intersystem crossing $\tilde{a}^4A'' \rightarrow X$ is weak due to the vanishingly small spin–orbit interactions. It further indicates that the direct dissociation on the $\tilde{a}^4A''$ state is more favored. This information combined with the comparison with isoelectronic HCCO provides an indirect support to the recent experimental proposal of photodissociation mechanism of HCNN.

Keywords CASSCF · CASPT2 · Quartet excited state · Photodissociation

1 Introduction

The HCNN radical has attracted considerable attention as a result of its important role in environment, atmospheric process, combustion reactions, and interstellar chemistry. The molecule was observed by Herzberg and Travis [1] for the first time. Then it attracted several interests in experimental studies [2–17]. One of them is that HCNN radical has been proved to be a chemical intermediate in the ground state reaction of CH with N_2 [5–17]. All the investigations focus on the following two reactions:

$$CH(\tilde{X}^2\Pi) + N_2(\tilde{X}^1\Sigma_g^+) \rightarrow HCN(\tilde{X}^1\Sigma^+) + N(^4S) \quad (1)$$

$$CH(\tilde{X}^2\Pi) + N_2(\tilde{X}^1\Sigma_g^+) \rightarrow NCN(\tilde{X}^3\Sigma_g^-) + H(^2S) \quad (2)$$

The two reactions are responsible for the formation of so-called "prompt NO", which was first discovered by Fenimore [5]. Cui et al. [15] used high-level ab initio electronic structure theories, such as CASSCF, CASPT2, CCSD(T), G2M(RCC), to investigate the reaction mechanism of the spin-forbidden reaction (1). By establishing detailed lowest-lying doublet and quartet potential energy surfaces (PES) of HCNN radical, they proposed that the dominant mechanism remains the C_{2v} intersystem-crossing step. After theoretical studies of the spin-allowed reaction (2), the fact that this reaction is more favorable to form the "prompt NO" than reaction (1) has been found by Moskaleva et al. [16] and further supported by Takayanagi [17].

In published assays, the infrared spectra of HCNN radical and photoelectron spectra of $HCNN^-$ were measured, but the absorptions were not assigned [3]. Theoretical study on two lowest-lying electronic states of HCNN radical, $\tilde{X}^2A''$ and $\tilde{A}^2A'$, proved that they are Renner–Teller pair having similar geometries and properties [18–21]. In photodissociation reactions, both of them correlate adiabatically with the ground state products CH ($\tilde{X}^2\Pi$) + $N_2(\tilde{X}^1\Sigma_g^+)$ without an exit barrier. In addition, less attention has been paid to higher electronic excited states both experimentally and theoretically.

More recently, Faulhaber et al. [22] first explored the photodissociation dynamics of HCNN radical using fast radical beam photofragment translational spectroscopy. A photofragment yield spectrum was obtained for the range of 25,510–40,820 cm^{-1} . Dissociation takes place following a

Y. Liu · X.-R. Huang (✉) · C.-C. Sun
State Key Laboratory of Theoretical and Computational Chemistry, Institute of Theoretical Chemistry, Jilin University, Changchun 130023, People's Republic of China
e-mail: quanchemly3@yahoo.com.cn

transition which is tentatively assigned as $\tilde{B} \leftarrow \tilde{X}^2A''$. All excitation energies studied lead to the formation of CH ($\tilde{X}^2\Pi$) and $N_2(\tilde{X}^1\Sigma_g^+)$ as the only detectable products. Since only the $\tilde{X}^2A''$ and $\tilde{A}^2A'$ states correlate with the ground state products, they proposed that the dissociation mechanism appears to involve internal conversion to one or both of the states.

As the isoelectronic radical, HCCO should have similar properties with HCNN radical. A detailed comparison for the photodissociation dynamics of the two radicals is much beneficial for us to study the properties of HCNN radical. The low-lying excited states PES of HCCO radical have been studied well. Plenty of earlier studies [23–27] showed that the photodissociation products of HCCO radical from the $\tilde{B}(^2\Pi)$ state have been identified as ground state fragments CH ($\tilde{X}^2\Pi$) + CO($\tilde{X}^1\Sigma^+$) via internal conversion, and excited state products CH ($\tilde{a}^4\Sigma^-$) + CO($\tilde{X}^1\Sigma^+$) via intersystem crossing. It implies that the quartet excited state PES played an important role in the photodissociation reactions of HCCO. However, the knowledge about the quartet excited state is scarce for HCNN radical. Here, we reported on extensive calculations of the quartet states PES of HCNN radical including the intersections with doublet $\tilde{X}^2A''$ and $\tilde{A}^2A'$ states, and the comparison with isoelectronic HCCO radical. This study thus is expected to be helpful to experimentally investigate the photodissociationions of HCNN radical.

2 Calculation details

All calculations are carried out by MOLCAS 6.2 program packages [28]. The stationary points on each given electronic state and the minimum energy crossing point (MECP) [29] on the surface of intersection are located by performing the complete active space self-consistent field (CASSCF) method. The CASSCF wavefunction can describe the multiconfiguration effect very well and has sufficient flexibility to model large changes of the electronic structure in dissociation reaction. We adopt the C_s symmetry in all the calculations. Once convergence reaches, the vibrational frequency is examined to confirm the stationary point to be a minimum or first-order saddle point. The intrinsic reaction coordinate (IRC) calculations at the CASSCF level are carried out to confirm the right connective relationship between the transition states and minima. Based on CASSCF optimized geometries, the second-order multiconfigurational perturbation theory (CASPT2) [30] single-point energy calculations with the same basis set and active space are performed to get reliable energy. The zero-point vibrational energies (ZPVE) at the CASSCF method are also included for energy correction. For the MECP structures, the CASPT2 energies with and without spin–orbit coupling (SOC) interactions [31] are obtained. Dunning's correlation consistent basis sets cc-pVDZ and cc-pVQZ, denoted as B1 and B2, respectively, are used throughout the calculations. The enlarged quadruple-zeta basis set is used to test the influence of basis set for the results.

Two sets of active spaces are selected for the calculations. One is all valence orbitals and electrons with the exception of the terminal atom nitrogen 2s and bond σ C–H, resulting in an active space of 11 active electrons with 12 active orbitals. The other set is made of full valence active space including 15 active electrons and 14 active orbitals. Although such large active space for this system is very time consuming, it is helpful for the precision of the results. Different basis sets and active spaces give rise to four kinds of methods, abbreviated to CAS(11/12)/B1, CAS(15/14)/B1, CAS(11/12)/B2, and CAS(15/14)/B2. Herein, we take the denoted CAS(11/12)/B1 as an example, which means that the geometries are optimized at the CASSCF method with cc-pVDZ basis set and active space of 11 active electrons and 12 active orbitals. Moreover, considering the CASPT2 single-point energies and ZPVE included, the labeling presenting the full calculations becomes CAS(11/12)PT2/B1, CAS(15/14)PT2/B1, CAS(11/12)PT2/B2, and CAS(15/14) PT2/B2, respectively.

3 Results and discussion

3.1 The quartet excited state $\tilde{a}^4A''$ PES

The ground state $\tilde{X}^2A''$ of HCNN radical and its Renner–Teller pair $\tilde{A}^2A'$ state have been treated by various theoretical calculations. The energy splitting range between the two states reported experimentally by Clifford et al. [19] is $0.522 \pm 0.012 - 0.675 \pm 0.012$ eV. Under our CAS(11/12) PT2/B1, CAS(15/14)PT2/B1, CAS(11/12)PT2/B2, and CAS (15/14)PT2/B2 methods, the corresponding results are 0.640, 0.620, 0.535, and 0.537 eV, respectively, which perfectly match with the experimental values. Their geometries listed in Table 1 are also in reasonable agreement with the results of Cui et al. [15]

In present study, we focus on the lowest-lying quartet PES of HCNN radical. The $\tilde{a}^4A''$ state has the predominant electronic configuration:

$$(\text{core})(4a')^2(5a')^2(6a')^2(7a')^2(8a')^2(9a')^1(10a')^1(1a'')^2(2a'')^1$$

The schematic $\tilde{a}^4A''$ PES is shown in Fig. 1. On the $\tilde{a}^4A''$ PES, two minima MINI-*cis* and MINI-*trans*, with *cis* and *trans* structures are obtained, respectively. The isomerization transition state with *trans* structure between them, TS-*iso*, is located. The slightly higher barrier of about 27 kcal/mol with the CAS(11/12)PT2/B1 method suggests that the two minima are difficult to convert into each other. Along the *cis* and *trans* reaction paths, two transition states TS-*cis* and TS-*trans* are

Table 1 Equilibrium geometries and relative energies of HCNN radical at CAS(11/12)PT2/B1, CAS(15/14)PT2/B1, CAS(11/12)PT2/B2, and CAS(15/14)PT2/B2 levels

	N–N (Å)	C–N (Å)	C–H (Å)	∠NNC (deg)	∠NCH (deg)	CASPT2 energy[a] (kcal/mol)	ZPVE[b] (kcal/mol)	Energy[c] (kcal/mol)	Reference
HCNN ($\tilde{X}^2A''$)									
CAS(11/12)PT2/B1	1.164	1.318	1.086	167.0	113.3	0.0	0.0	0.0	This work
CAS(15/14)PT2/B1	1.168	1.311	1.115	167.8	111.6	0.0	0.0	0.0	This work
CAS(11/12)PT2/B2	1.144	1.310	1.103	168.2	108.9	0.0	0.0	0.0	This work
CAS(15/14)PT2/B2	1.155	1.302	1.103	168.6	112.1	0.0	0.0	0.0	This work
B3LYP/6-311G(d,p)	1.155	1.274	1.089	169.9	115.5	0.0	0.0	0.0	[15][d]
HCNN ($\tilde{A}^2A'$)									
CAS(11/12)PT2/B1	1.188	1.254	1.069	173.7	140.2	14.7	0.1	14.8	This work
CAS(15/14)PT2/B1	1.188	1.253	1.090	174.3	139.9	14.0	0.3	14.3	This work
CAS(11/12)PT2/B2	1.181	1.239	1.057	174.0	142.5	11.8	0.5	12.3	This work
CAS(15/14)PT2/B2	1.180	1.240	1.079	174.5	141.4	12.0	0.4	12.4	This work
CASSCF/6-311G(d,p)	1.176	1.235	1.059	173.9	141.4	13.5		12.5	[15]
MINI-*cis* ($\tilde{a}^4A''$)									
CAS(11/12)PT2/B1	1.247	1.355	1.110	121.5	130.6	39.4	−1.1	38.3	This work
CAS(15/14)PT2/B1	1.249	1.344	1.111	123.7	130.6	38.3	−0.5	37.8	This work
CAS(11/12)PT2/B2	1.239	1.345	1.073	123.4	129.7	41.0	−0.1	40.9	This work
CAS(15/14)PT2/B2	1.246	1.340	1.086	123.7	130.4	42.5	0.0	42.5	This work
B3LYP/6-311G(d,p)	1.248	1.297	1.093	125.8	131.0	47.8	−0.5	47.3	[15]
MINI-*trans* ($\tilde{a}^4A''$)									
CAS(11/12)PT2/B1	1.269	1.342	1.081	117.3	125.0	39.2	−0.5	38.7	This work
CAS(15/14)PT2/B1	1.267	1.341	1.104	117.0	125.3	38.4	−1.3	37.1	This work
CAS(11/12)PT2/B2	1.259	1.336	1.070	117.8	125.4	40.7	−0.1	40.6	This work
CAS(15/14)PT2/B2	1.257	1.334	1.092	117.5	125.7	42.2	0.2	42.4	This work
B3LYP/6-311G(d,p)	1.265	1.294	1.085	119.7	127.1	48.1	−0.4	47.7	[15]
TS-*iso* ($\tilde{a}^4A''$)									
CAS(11/12)PT2/B1	1.265	1.303	1.101	175.7	125.2	67.4	−1.8	65.6	This work
CAS(15/14)PT2/B1	1.271	1.296	1.109	175.3	125.6	68.3	−1.7	66.6	This work
CAS(11/12)PT2/B2	1.254	1.272	1.124	175.6	125.2	69.6	−1.8	67.8	This work
CAS(15/14)PT2/B2	1.262	1.286	1.096	175.8	125.9	70.4	−1.5	68.9	This work
B3LYP/6-311G(d,p)	1.252	1.268	1.122	175.1	126.1	76.5	−2.0	74.5	[15]
TS-*cis* ($\tilde{a}^4A''$)									
CAS(11/12)PT2/B1	1.160	1.686	1.110	121.9	136.8	56.5	−2.4	54.1	This work
CAS(15/14)PT2/B1	1.162	1.657	1.110	125.1	133.2	55.3	−2.1	53.2	This work
CAS(11/12)PT2/B2	1.143	1.714	1.076	124.6	136.2	61.3	−1.6	59.7	This work
CAS(15/14)PT2/B2	1.146	1.682	1.099	125.3	138.5	61.7	−2.6	59.1	This work
B3LYP/6-311G(d,p)	1.115	1.883	1.098	129.5	151.0	66.6	−2.5	64.1	[15]
TS-*trans* ($\tilde{a}^4A''$)									
CAS(11/12)PT2/B1	1.167	1.718	1.106	109.3	128.5	57.9	−2.5	55.4	This work
CAS(15/14)PT2/B1	1.164	1.715	1.105	111.4	132.0	56.9	−2.2	54.7	This work
CAS(11/12)PT2/B2	1.148	1.741	1.070	111.5	128.8	62.9	−1.8	61.1	This work
CAS(15/14)PT2/B2	1.152	1.713	1.093	111.9	131.3	63.7	−2.2	61.5	This work
B3LYP/6-311G(d,p)	1.121	1.896	1.093	112.3	143.8	70.6	−2.9	67.7	[15]

[a] The CASPT2 single-point energies of the reference structure HCNN($\tilde{X}^2A''$) at CAS(11/12)PT2/B1, CAS(15/14) PT2/B1, CAS(11/12) PT2/B2, and CAS(15/14) PT2/B2 are −147.6810516388, −147.6853164074, −147.9326265532, and −147.9369082107 a.u., respectively

[b] The ZPVE of the reference structure HCNN($\tilde{X}^2A''$) at CAS(11/12)/B1, CAS(15/14)/B1, CAS(11/12)/B2, and CAS(15/14)/B2 are 11.75, 11.24, 11.25, and 11.20 kcal/mol, respectively

[c] The energy is equal to the CASPT2 energy plus ZPVE for each structure

[d] The relative energies in [15] are calculated with G2M(RCC), including B3LYP/6-311g(d,p) zero-point energy. They are deduced from Fig. 4 and Table 1 of [15]

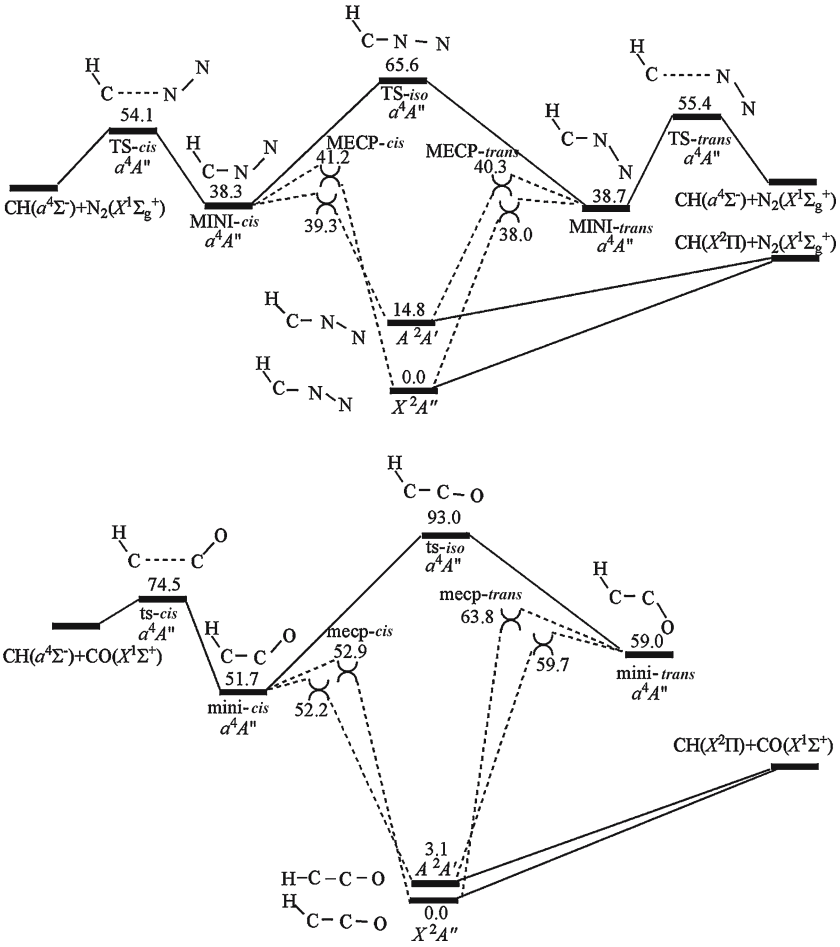

Fig. 1 The schematic potential energy surfaces of HCNN and HCCO including the low-lying electronic states at the CAS(11/12)PT2/B1 level. The relative energies are in kcal/mol

located, respectively. The elongated C–N bond along with the analysis for the vibrational frequencies of the transition states indicates the trend of C–N bond dissociation. The following IRC calculations with the CAS(11/12)/B1 method further confirm that they correlate to the MINI-*cis* and MINI-*trans* as the reactant side, respectively. After checking the reaction path from the point of view of electron structure on the products side, we use the components of molecular orbitals to express the product side of IRC calculation as follows.

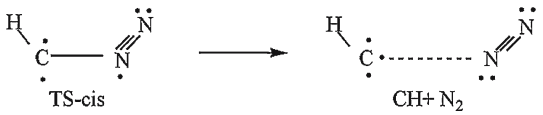

The symbols "•", "••", and "–" represent the single electron, lone pairs electrons, and chemical bond, respectively. The total of the net Mulliken charge populations on C and H atoms becomes nearly 0.00 when the C–N bond length comes to 3.0 Å. Therefore, the products correspond to neutral CH and N_2 molecules. The dominant configuration state functions of products are $(\text{core})(4a')^2(5a')^2(6a')^2(7a')^2(8a')^2(9a')^{\text{u}}(10a')^{\text{u}}(1a'')^2(2a'')^{\text{u}}$ with the CI-coefficient of 0.96, (the "2" means the full-occupied number, the "u" means single occupation with spin up). But the three singlet occupational orbitals have turned to the P_x, P_y, P_z orbitals of C atom. We can easily reach the conclusion from the facts above to confirm that the products are CH ($\tilde{a}^4\Sigma^-$) and $N_2(\tilde{X}^1\Sigma_g^+)$. Similar conclusion could be reached from the *trans* dissociation path as follows; thus, detail information will be unnecessary at this point.

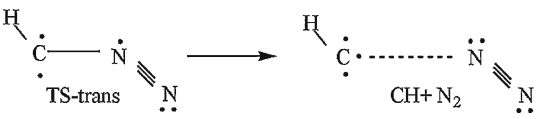

Note that all the energy values on the PES are relatively referenced to ground state HCNN ($\tilde{X}^2A''$) under different methods. It shows that the barrier of the *cis* dissociation path from the MINI-*cis* comes to 15.8, 15.4, 18.8, and 16.6 kcal/mol under CAS(11/12)PT2/B1, CAS(15/14) PT2/B1, CAS(11/12)PT2/B2, and CAS(15/14)PT2/B2 levels, respectively. The *trans* dissociation path has a little higher barrier, i.e. 16.7, 17.6, 20.5, and 19.1 kcal/mol, under CAS (11/12)PT2/B1, CAS(15/14)PT2/B1, CAS(11/12) PT2/B2,

and CAS(15/14) PT2/B2 levels, respectively. The energies and geometries of the minima and transition states on $\tilde{a}^4A''$ PES under above four methods are listed in Table 1. Agreement is quite good among the results of the four methods. The geometry parameters change less than 0.1 Å in bond length, and 5.0° in bond angle, and the energies change considerably little as well. The enlarged active space and basis set have trivial influence for the results. Especially, the influence of the active space on the results is much smaller than that of basis set. It implies that the CAS(11/12)PT2/B1 method with the relative small active space and basis set is credible enough for present theoretical estimates.

Little work on the $\tilde{a}^4A''$ PES of HCNN was performed. In 1999, Cui et al. [15] studied the role of the $\tilde{a}^4A''$ PES in the spin-forbidden reaction $CH(^2\Pi)+N_2 \rightarrow HCN+N(^4S)$. As shown in Fig. 4 of [15], their study focused on the C_{2v} surface crossings, but the present work cares more on the states on the left side of that figure. Some stationary points related to C–N bond dissociation path were located, but a few were discussed. The corresponding values with B3LYP and G2M(RCC) methods are also listed in Table 1. In contrast, their relative energies are much higher than those presented in above four methods. The differences of energies are by 10 kcal/mol at most, which are reasonable with different calculation methods and basis sets.

3.2 The nonadiabatic interactions

To investigate the quartet state $\tilde{a}^4A''$ PES of HCNN radical in detail, much attention should be devoted to the nonadiabatic interactions between $\tilde{a}^4A''$ and low-lying X ($X = \tilde{X}^2A''$ and $\tilde{A}^2A'$) states. The photochemical reactions usually relate to different PES and the intersection region where the system decays from one state to another. Therefore, the minimum energy crossing points (MECP) on a surface of intersection are efficient routes to reveal the reaction mechanism.

After exhaustive searches, four MECP between $\tilde{a}^4A''$ and X ($X = \tilde{X}^2A''$ and $\tilde{A}^2A'$) surfaces of intersection are obtained. As shown in Fig. 2, the optimized geometries of those MECP are consistent with the CAS(11/12)/B1, CAS(15/14)/B1, CAS(11/12)/B2, and CAS(15/14)/B2 methods. It is worth mentioning that the geometries of the MECP-*cis* and MECP-*trans* between $\tilde{a}^4A''$ and X (X=$\tilde{X}^2A''$ and $\tilde{A}^2A'$) states are similar to MINI-*cis* and MINI-*trans* on $\tilde{a}^4A''$ PES, respectively. Furthermore, the energies of the MECP are considerably close to that of MINI-*cis* and MINI-*trans*. It is well accepted that at the MECP structures optimized by the CASSCF method, the CASPT2 solution splits will more or less break the degeneracy between the states. In this case that both the degenerate states have the same characteristics, i.e., valence states, the dynamic correlation is usually the same. For present study, we found that the energy splits are much more trivial, and then the single point energy on quartet state is identified to present the CASPT2 solution for all the MECP structures. Under the CAS(11/12)PT2/B1 method, the energies of the four MECP range from 38.0 to 41.2 kcal/mol. So all the MECP are located near to the minimum structures on the $\tilde{a}^4A''$ PES of HCNN, clearly shown in Fig. 1.

The nonadiabatic interactions through the surface of intersection and direct dissociation through transition states are competitive pathways in the photodissociation process. If the energies of MECP exceed those of transition states, the intersystem crossing hardly happen. For the present case, the MECP are located far lower than the transition states on the $\tilde{a}^4A''$ PES. Thus, from the aspect of the energy, the surface of intersection is more favorable. However, when it is energetically accessible, the MECP alone is not sufficient. The spin–orbit interactions have a special meaning for photochemistry, since it is responsible for spin-forbidden electronic transition. To be continued, we will discuss the spin–orbit interactions between the quartet and doublet states.

Many methods have been used to analyze the spin–orbit interactions (H^{so}). Here we report how much the spin–orbit coupling changes the energies of the two crossing electronic states at the MECP structure. This is the most essential method, because the spin–orbit coupling interactions eventually cause the change of energy. We obtain the energies with and without SOC at the MECP geometries. From the results, we can find that the energy change with and without SOC on the assigned spin-free state, i.e., $\tilde{a}^4A''$, $\tilde{X}^2A''$, or $\tilde{A}^2A'$ state, is trivial and may be ignored. Even the change of the energy differences (ΔE) between the crossing states with and without SOC is less than 2 cm^{-1} . It shows weak spin–orbit interactions and little possibility of converting to the $\tilde{X}^2A''$ and $\tilde{A}^2A'$ states from the $\tilde{a}^4A''$ state through the MECP structures.

In summary, on the $\tilde{a}^4A''$ state of HCNN radical, the intersystem crossing to $\tilde{X}^2A''$ and $\tilde{A}^2A'$ states hardly happens because of weak spin–orbit interactions; therefore, the direct dissociation to CH ($\tilde{a}^4\Sigma^-$) and N_2 ($\tilde{X}^1\Sigma_g^+$) with slightly low barrier dominates the reaction on the $\tilde{a}^4A''$ state of HCNN radical. But comparing isoelectronic HCCO as listed in the following is preferred.

3.3 Comparison with HCCO radical

As an isoelectronic radical, HCCO should have comparable properties on the $\tilde{a}^4A''$ PES with HCNN radical. Most importantly, both experiment and theoretical calculations showed that HCCO radical could obtain quartet state products CH ($\tilde{a}^4\Sigma^-$) + CO ($\tilde{X}^1\Sigma^+$). Although it has been well studied, we still could refine and supply the $\tilde{a}^4A''$ PES of HCCO radical with the present CAS(11/12)PT2/B1 method. Our results show that it is similar to that established by Yarkony [25] with the SA-MCSCF method, as shown in Table 2 and Fig. 1. Two

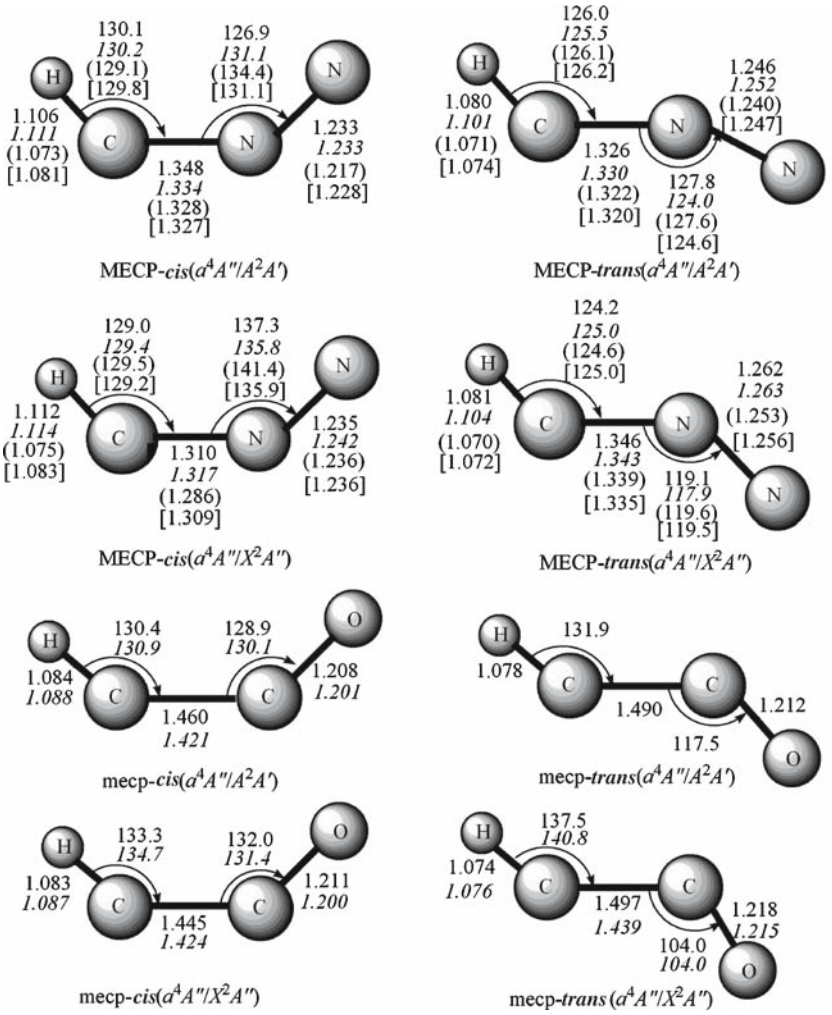

Fig. 2 The optimized geometries of the MECP on the ($\tilde{a}^4A''$ /$\tilde{X}^2A''$ or $\tilde{A}^2A'$) surface of intersection of HCNN and HCCO radical. Bond lengths are in angstroms and angles are in degrees. For HCNN, the values in *regular, italics, parentheses*, and *brackets* are at CAS(11,12)/B1, CAS(15/14)/B1, CAS(11/12)/B2, and CAS(15/14)/B2 levels, respectively. For HCCO, the values in *regular* and *italics* are at our CAS(11,12)/B1 and referenced SA-MCSCF/DZP [25] methods, respectively

minima and two transition states with planar structures are located. The isomerization transition state, ts-*iso*, is found to relate to the minima mini-*cis* and mini-*trans*, and the barrier height has come to 41.3 kcal/mol from the mini-*cis*. To our knowledge, no reports have been found in the literature on the isomerization transition state up to now. The other transition state ts-*cis* is on the dissociation path to CH ($\tilde{a}^4\Sigma^-$) and CO ($\tilde{X}^1\Sigma^+$) with barrier of 22.8 kcal/mol from the mini-*cis*. As shown in Fig. 1, it is obvious that the dissociation barrier of HCCO radical is 7.0 kcal/mol higher than that of HCNN radical. If we only consider the barrier height, the dissociation reaction of HCNN on $\tilde{a}^4A''$ PES is more feasible than that of HCCO.

With the CAS(11/12)/B1 method, we also locate the MECP between $\tilde{a}^4A''$ and $X(X = \tilde{X}^2A''$ and $\tilde{A}^2A')$ surfaces of HCCO radical, as shown in Figs. 1, 2. They are also located around the mini-*cis* and mini-*trans* structures. The located MECP on a surface of intersection have similar geometries with those of Yarkony [25]. Just the MECP with *trans* structure between the $\tilde{a}^4A''$ and $\tilde{A}^2A'$ states is new finding. Moreover, Yarkony concluded that the spin–orbit interactions at the MECP between $\tilde{a}^4A''$ and $X(X = \tilde{X}^2A''$ and $\tilde{A}^2A')$ states are so strong that they play a significant role in the quenching process. As HCNN radical, we calculated the energies with and without SOC at the MECP geometries of HCCO radical. The results show that the change of energy difference (ΔE) between the two crossing states with and without SOC comes to 18.3 cm^{-1} at most. Furthermore, the energy changes with and without SOC for the particular spin-free state are also larger than these of HCNN. All those indicate much stronger spin–orbit interactions between $\tilde{a}^4A''$ and $X(X = \tilde{X}^2A''$ and $\tilde{A}^2A')$ states of HCCO than those of HCNN radical.

Therefore, we can conclude that compared with the HCCO radical, the HCNN radical on the $\tilde{a}^4A''$ state shows more tendency to dissociate, because of much lower dissociation barrier and weaker nonadiabatic interactions with $\tilde{X}^2A''$ and $\tilde{A}^2A'$ states. Then we could predict that in the photodissociation process, if HCNN falls down to the $\tilde{a}^4A''$ state from initial $\tilde{B}$ state through intersystem crossing, it must lead to the quartet state products CH ($\tilde{a}^4\Sigma^-$) and $N_2(\tilde{X}^1\Sigma_g^+)$. However, only ground states products CH ($\tilde{X}^2\Pi$) and $N_2(\tilde{X}^1\Sigma_g^+)$ were

Table 2 Equilibrium geometries and energies of HCCO radical at CAS(11/12)PT2/B1 level

	O–C (Å)	C–C (Å)	C–H (Å)	∠OCC (deg)	∠CCH (deg)	CASPT2 Energy[a] (kcal/mol)	ZPVE[b] (kcal/mol)	Energy[c] (kcal/mol)	Reference
HCCO($\tilde{X}^2A''$)									
CAS(11/12)PT2/B1	1.188	1.327	1.074	167.5	131.4	0.0	0.0	0.0	This work
SA-MCSCF/DZP	1.181	1.313	1.076	167.2	131.1	0.0			[25]
HCCO($\tilde{A}^2A'$)									
CAS(11/12)PT2/B1	1.204	1.280	1.061	180.0	180.0	3.2	−0.1	3.1	This work
SA-MCSCF/DZP	1.195	1.264	1.064	180.0	180.0	5.3			[25]
mini-*cis* ($\tilde{a}^4A''$)									
CAS(11/12)PT2/B1	1.207	1.481	1.084	125.4	130.5	51.9	−0.2	51.7	This work
SA-MCSCF/DZP	1.198	1.445	1.088	125.5	131.2	52.2			[25]
mini-*trans* ($\tilde{a}^4A''$)									
CAS(11/12)PT2/B1	1.212	1.481	1.078	119.9	131.9	59.6	−0.6	59.0	This work
SA-MCSCF/DZP	1.203	1.444	1.080	120.0	134.3	59.8			[25]
ts-*iso* ($\tilde{a}^4A''$)									
CAS(11/12)PT2/B1	1.223	1.449	1.095	175.4	125.0	94.3	−1.3	93.0	This work
ts-*cis* ($\tilde{a}^4A''$)									
CAS(11/12)PT2/B1	1.150	1.916	1.109	126.0	149.2	77.4	−2.9	74.5	This work
SA-MCSCF/DZP	1.141	2.121	1.093	128.3	156.3	82.9			[25]

[a] The CASPT2 single-point energy of the reference structure HCCO($\tilde{X}^2A''$) at CAS(11/12)PT2/B1 method is −151.5228471487 a.u
[b] The ZPVE of the reference structure HCCO($\tilde{X}^2A''$) at the CAS(11/12)/B1 method is 12.01 kcal/mol
[c] The energy is equal to the CASPT2 energy plus ZPVE for each structure

detected in recent experimental investigations by Faulhaber et al. [22]. Thus, we can easily reach the conclusion that the intersystem crossing between the $\tilde{B}$ and $\tilde{a}^4A''$ states would not be involved in the photodissociation mechanism of HCNN radical. It is in good agreement with the experimental proposal by Faulhaber et al. [22] that no evidence for intersystem crossing has been detected in the photodissociation dynamics of HCNN. Once this path is excluded, the other main path of internal conversion to one or both the $\tilde{X}^2A''$ and $\tilde{A}^2A'$ states must be involved in the photodissociation mechanism of HCNN radical. Based on the information on the $\tilde{a}^4A''$ state PES of HCNN above, combined with the comparison with isoelectronic HCCO radical, we deduced indirectly the experimental photodissociation mechanism. As for the direct proof about that, it need further study in future. The results reported here provide useful information for the experimental investigations of HCNN radical.

4 Conclusion

We have investigated the quartet excited state $\tilde{a}^4A''$ PES of HCNN radical utilizing CASSCF and CASPT2 methods. Two minima and three transition states are located. It shows that the direct dissociation to CH ($\tilde{a}^4\Sigma^-$) and $N_2(\tilde{X}^1\Sigma_g^+)$ with slightly low barrier dominates the reaction on the $\tilde{a}^4A''$ state of HCNN radical. While there is little possibility for a process from $\tilde{a}^4A''$ to $\tilde{X}^2A''$ and $\tilde{A}^2A'$ states via an intersystem crossing because of weak nonadiabatic interactions. Additionally, the $\tilde{a}^4A''$ PES of isoelectronic HCCO radical is depicted for comparison with HCNN. It indicates that compared with HCCO, HCNN radical on the $\tilde{a}^4A''$ state shows more tendency to dissociate to CH ($\tilde{a}^4\Sigma^-$) and $N_2(\tilde{X}^1\Sigma_g^+)$, due to much lower dissociation barrier and weaker spin–orbit coupling interactions with $\tilde{X}^2A''$ and $\tilde{A}^2A'$ states. The present study provides an indirect support to the experimental proposal of photodissociation mechanism that internal conversion to one or both of the $\tilde{X}^2A''$ and $\tilde{A}^2A'$ states, instead of intersystem crossing, is involved in the photodissociation mechanism of HCNN radical.

Acknowledgments This work is supported by the National Nature Science Foundation of China (No. 20333050, 20643004), Excellent Young Foundation of Jilin Province, and Technology Development Project of Jilin Province (20050906-6). The authors are greatly thankful for the reviewers' invaluable comments.

References

1. Herzberg G, Travis DN (1964) Can J Phys 42:1658
2. Basco N, Yee KK (1968) Chem Commun (Camb) 3:150
3. Ogilvie JF (1968) Can J Chem 46:2472
4. Kroto HW, Morgan TF, Sheena HH (1970) Trans Faraday Soc 66:2237

5. Fenimore CP (1971) In: 13th symposium (International) on combustion. The Combustion Institute, Pittsburgh, p 373
6. Berman MR, Lin MC (1983) J Phys Chem 87:3933
7. Miller JA, Bowman CT (1989) Prog Energy Combust Sci 15:287
8. Medhurst LJ, Garland NL, Nelson HH (1993) J Phys Chem 97:12275
9. Fulle D, Hippler H (1996) J Chem Phys 105:5423
10. Le Picard SD, Canosa A, Rowe BR, Brownsword RA, Smith IWM (1998) J Chem Soc Faraday Trans 94:2889
11. Manaa MR, Yarkony DR (1991) J Chem Phys 95:1808
12. Manaa MR, Yarkony DR (1992) Chem Phys Lett 188:352
13. Martin JML, Taylor PR (1993) Chem Phys Lett 209:143
14. Seideman T, Walch SP (1994) J Chem Phys 101:3656
15. Cui Q, Morokuma K (1999) Theor Chem Acc 102:127
16. Moskaleva LV, Xia WS, Lin MC (2000) Chem Phys Lett 331:269
17. Takayanagi T (2003) Chem Phys Lett 368:393
18. Thomson C (1973) J Chem Phys 58:841
19. Clifford EP, Wenthold PG, Lineberger WC, Petersson GA, Broadus KM, Kass SR, Kato S, DePuy CH, Bierbaum VM, Ellison GB (1998) J Phys Chem A 102:7100
20. Fleming PE (2000) Chem Phys Lett 321:129
21. Puzzarini C, Gambi A (2005) J Chem Phys 122:064316
22. Faulhaber AE, Gascooke JR, Hoops AA, Neumark DM (2006) J Chem Phys 124:204303
23. Hu CH, Schaefer HF, Hou Z, Bayes KD (1993) J Am Chem Soc 115:6904
24. Szalay PG, Fogarasi G, Nemes L (1996) Chem Phys Lett 263:91
25. Yarkony D (1996) J Phys Chem 100:17439
26. Mordaunt DH, Osborn DL, Choi H, Bise RT, Neumark DM (1996) J Chem Phys 105:6078
27. Osborn DL, Mordaunt DH, Choi H, Bise RT, Neumark DM, Rohlfing CM (1997) J Chem Phys 106:10087
28. Karlström G, Lindh R, Malmqvist P-Å, Roos BO, Ryde U, Veryazov V, Widmark P-O, Cossi M, Schimmelpfennig B, Neogrady P, Seijo L (2003) Comput Mater Sci 28:222
29. De Vico L, Olivucci M, Lindh R (2005) J Comp Theor Chem 1:1029
30. Andersson K, Malmqvist P-Å, Roos BO, Sadlej AJ, Wolinski K (1990) J Phys Chem 94:5483
31. Hess BA, Marian CM, Wahlgren U, Gropen O (1996) Chem Phys Lett 251:365